applied sciences

MDPI

Article

Temporal Convolutional Network-Based Axle Load Estimation from Pavement Vibration Data

Zeying Bian [1,2], Mengyuan Zeng [1,2,3,*], Hongduo Zhao [1,2], Mu Guo [1,2] and Juewei Cai [4]

[1] Key Laboratory of Road and Traffic Engineering, Ministry of Education, Tongji University, Shanghai 201804, China; zybian@tongji.edu.cn (Z.B.); hdzhao@tongji.edu.cn (H.Z.); guomu.zest@foxmail.com (M.G.)
[2] The Key Laboratory of Infrastructure Durability and Operation Safety in Airfield of CAAC, Tongji University, Shanghai 201804, China
[3] Department of Civil, Environmental and Geomatic Engineering, ETH Zurich, 8093 Zurich, Switzerland
[4] Shanghai Research Institute of Building Sciences Co., Ltd., Shanghai 201108, China; jueweicai@126.com
* Correspondence: myzeng@tongji.edu.cn

Abstract: Measuring the axle loads of vehicles with more accuracy is a crucial step in weight enforcement and pavement condition assessment. This paper proposed a vibration-based method, which has an extended sensing range, high temporal sampling rate, and dense spatial sampling rate, to estimate axle loads in concrete pavement using distributed optical vibration sensing (DOVS) technology. Temporal convolutional networks (TCN), which consist of non-causal convolutional layers and a concatenate layer, were proposed and trained by over 6000 samples of vibration data and ground truth of axle loads. Moreover, the TCN could learn the complex inverse mapping between pavement structure inputs and outputs. The performance of the proposed method was calibrated in two field tests with various conditions. The results demonstrate that the proposed method obtained estimated axle loads within 11.5% error, under diverse circumstances that consisted of different pavement types and loads moving at speeds ranging from 0~35 m/s. The proposed method demonstrates significant promise in the field of axle load reconstruction and estimation. Its error, closely approaching the 10% threshold specified by LTPP, underscores its efficacy. Additionally, the method aligns with the standards set by Cost-323, with an error level-up to category C. This indicates its capability to provide valuable support in the assessment and decision-making processes related to pavement structure conditions.

Keywords: weigh in motion; axle load estimation; pavement vibration; temporal convolutional networks; distributed optical vibration sensing

Citation: Bian, Z.; Zeng, M.; Zhao, H.; Guo, M.; Cai, J. Temporal Convolutional Network-Based Axle Load Estimation from Pavement Vibration Data. *Appl. Sci.* **2023**, *13*, 13264. https://doi.org/10.3390/app132413264

Academic Editor: Luís Picado Santos

Received: 31 October 2023
Revised: 2 December 2023
Accepted: 6 December 2023
Published: 14 December 2023

1. Introduction

Capturing vehicle axle weight is crucial in weight enforcement and assessing pavement condition. Accurate axle load estimates assist in regulatory compliance, targeted inspections, load-induced pavement damage assessment, pavement design and planning, and optimized maintenance scheduling [1–3]. Weigh in motion (WIM) is an efficient method for measuring axle weight while a vehicle is moving at normal speed. Traditional WIM systems use load cells, bending plates, and piezoelectric sensors [4–7] to measure the pressure between tires and the road. However, these sensors are not only expensive but also impractical when vehicles drive too fast, as there is insufficient time to register changes in pressure. Furthermore, these sensors must be installed on the road surface, and the connection between sensors and road structures deteriorates under repeated traffic loads, leading to increasing measurement errors [8].

Vibration-based weigh-in-motion methods have gained popularity in recent years, as traffic-induced pavement vibration contains valuable information on traffic loads and pavement structure. The measured vibration data can be utilized for traffic monitoring [9,10]

and structural health monitoring [11,12] through vibration analysis. Ye et al. [13] developed acceleration sensing nodes to measure pavement vibration and identified abnormal axle weights based on the collected vibration data. Bajwa et al. [14] developed a cost-effective MEMS accelerometer to measure traffic-induced vibration and estimate the axle weights of trucks. Vibration sensors have a sampling frequency of up to 512 Hz, which is more appropriate than pressure sensors at high speeds.

However, there are challenges associated with vibration-based WIM methods. Firstly, pavement vibrations attenuate when transmitted over a distance due to damping [15,16], leading to low signal-to-noise ratio (SNR) measurements when traffic loads are too far away from the vibration sensor. Moreover, conventional vibration sensors are single-point sensors with limited spatial measurement range, making it challenging to ensure that moving tires are located exactly on those sensors [17,18]. Secondly, pavement vibrations are related to pavement conditions, requiring the removal of structural effects during vibration analysis. The process is based on vibration characteristics in the time and frequency domains, such as frequency response functions, modal coordinates [19–21], convolution integrals, and transfer functions [22–24], which typically require complicated mathematical modeling and formula derivation. Thus, analyzed results are susceptible to measurement noise and mathematical model errors [25,26].

Distributed optical vibration sensing (DOVS) technology provides a promising solution to overcome these challenges. DOVS-based vibration sensing systems can measure traffic-induced vibration with a high sampling frequency and precise location accuracy. Zhao et al. [27] developed a DOVS-based vibration sensing system to estimate the category of vehicles and load level through time–frequency analysis. Zeng et al. [28–31] utilized DOVS to reconstruct vehicle-induced vibration and analyze the modal characteristics of concrete pavement to recognize damage. Ye et al. [32,33] proposed a data processing method for this system, which included denoising and cutting vibration periods. The processed data are utilized to estimate the speed, position, and category of vehicles. For vibration analysis, recurrent neural networks (RNNs) are well suited for investigating the complex nonlinear relationship between input and output data through a training process [34–37]. Compared to traditional RNNs, temporal convolutional networks (TCN) have equivariance properties and sparse interactions that translate well into the time domain. The infinite memory advantage of RNNs is largely absent in practice. TCN exhibit longer memory than recurrent architectures with the same capacity. A thorough comparison by Bai et al. [38] demonstrated that TCN convincingly outperformed RNNs on various sequence modeling tasks.

In this paper, we present a vibration-based method to estimate axle weights using DOVS and TCN. We first utilize a DOVS-based vibration sensing system and a data preprocessing process to acquire pavement vibration signal datasets. Then, we propose a deep learning-based method to reconstruct and estimate axle loads. To validate our method, we performed a series of experiments that tested the performance of estimating load with various load conditions and cement concrete pavement.

The main innovations of this paper are as follows:

- A pavement vibration acquisition method based on distributed optical vibration sensors (DOVS) is developed;
- A deep learning-based load reconstruction method tailored for pavement vibration data collected by DOVS is proposed.

The remainder of this paper is organized as follows: First, a methodology is developed in Section 2, including data acquisition, schematics of algorithms, training strategies, and performance metrics. Second, conducted field tests are described in Section 3. The DOVS-based vibration sensing systems were employed in two different cases and other sensors were utilized to measure the ground truth of axle weights. In Section 4, the results of different traffic loads and pavement structures are compared and discussed.

2. Methods

This section presents the sequence-to-sequence method for estimating axle loads using DOVS and TCN. The method's overview is depicted in Figure 1. Firstly, data acquisition, preprocessing, and augmentation were carried out, wherein a sufficient amount of data, comprising vibration signals from DOVS and load–time curves, were collected from the experiment. The original data were then subjected to filtering, normalization, down-sampling, and random window selection. Next, the preprocessed data were partitioned into training, validation, and testing samples. Subsequently, a TCN-based network was constructed and trained to handle various types of axle load estimation tasks. Finally, the network's performance was verified and applied to estimate the tested moving loads.

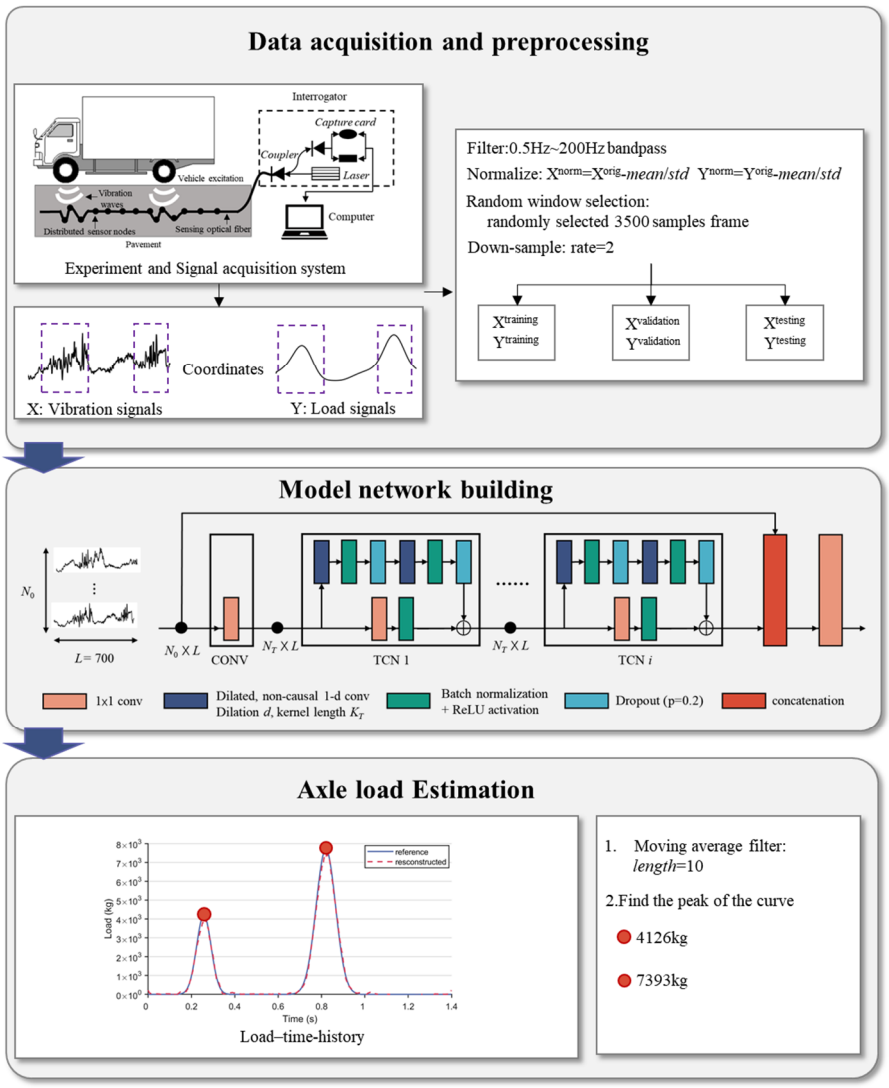

Figure 1. The overview of the proposed TCN-based method for axle load estimation.

2.1. Data Acquisition

In this paper, we utilized a DOVS-based vibration sensing system to acquire the original pavement vibration signal with a higher spatial resolution (see Figure 1: data acquisition and preprocessing). DOVS technology uses the principle of phase optical time-domain reflection (φ-OTDR), which allows a single fiber optic cable to function as a multipoint sensor for measurement and localization. The schematic principle of φ-OTDR is illustrated in Figure 1. During measurement, the measurement device emits pulsed light continuously at one end of the cable, and the light waves reflect the signal continuously to the device along the cable's axis. The position information of the measurement channel can

be analyzed according to the time difference of each reflected light. When a vibration event disturbs the cable, its mechanical properties in the section change, affecting the scattered amplitude of the reflected light. Therefore, the relative amplitude of the reflected light can be used to analyze the vibration information. Consequently, through the distributed optical vibration sensor, we can measure the vibration along the fiber optic cable at different time instances.

The fiber optic sensing data typically contain a significant number of redundant signals, which need to be processed before analysis. Moreover, the vibration data must be extracted from the raw data by selecting the appropriate time window for analysis. The vibration data are extracted from raw signals through anomaly detection based on a Gaussian model of the noise signal. Figure 2 shows the vibration signal detection algorithm. First, the sensing data are collected from different channels. Then, the short-time energy of each data frame is calculated as defined by (1). A Gaussian noise model is built based on the short-time energy of a series of noise signal segments collected, according to (2) and (3), to estimate the model parameters. The short-time energy noise signal was tested for Gaussianity using a quantile–quantile plot as depicted in Figure 2 (noise probability models part). The majority of the samples align with the line. When new data are detected, the short-time energy of the signal is calculated and compared with the Gaussian model. If the signal energy surpasses a threshold of 3σ, the corresponding signal frame is considered an anomalous segment containing the vibration signal. Consecutive windows containing vibration signals are merged. The decision of whether to record the signal or not is based on whether the number of channels with vibration detection exceeds a ratio of the total number of channels determined by the spatial distribution of signal energy. On the other hand, when a signal frame is detected as noisy, it is incorporated into a series of previous noisy signal frames. The system updates the Gaussian model of noise so that the model can accommodate different noise levels at different times of the day.

$$E_i(n) = \sum_{t=0}^{\infty} [x_i(t)\omega(t-n)]^2 \tag{1}$$

$$\omega(t-n) = \begin{cases} 1, & n \le i \le M+n \\ 0, & otherwise \end{cases} \tag{2}$$

$$\mu_i = \frac{1}{N}\sum_{n=0}^{N} E_i(n)^2 \tag{3}$$

$$\sigma_i = \frac{1}{N-1}\sum_{n=0}^{N} (E_i(n) - \mu_i)^2 \tag{4}$$

where $E_i(n)$ is the short-time energy of the nth frame, x_i is the vibration signals at channel I, $\omega(t-n)$ is a rectangular windows function expressed as (2), μ_i is the mean value of the Gaussian model corresponding to the ith channel, and σ_i is the standard deviation value of the Gaussian model corresponding to the ith channel.

2.2. Data Preprocessing

Zeng et al. [28] developed a pavement vibration sensing system using distributed optical vibration sensing technology. A fiber cable was looped in a vibration sensing system, providing a positioning accuracy of 0.3 m and a sampling frequency of 2500 Hz. In this study, a DOVS-based vibration sensing system was utilized to measure traffic-induced vibration by embedding it into a pavement structure.

To enhance the quality of the data, several steps were taken, including filtering, normalization, down-sampling, and window selection. According to Yuan et al. [39], surface waves induced by passing vehicles have concentrated energy in the frequency band of 0.5 Hz to 200 Hz. Low-frequency energy corresponds to quasi-static deformation caused by the weight of vehicles. Thus, 0.5 Hz to 200 Hz bandpass Butterworth filters were applied

for noise reduction. Random windows of length 3500 were selected, and the signal was down-sampled by a factor of 5 to reduce network parameters. Figure 1 shows the details of the data preprocessing process. These steps aimed to expand the data set, improve the signal-to-noise ratio, and accelerate network convergence.

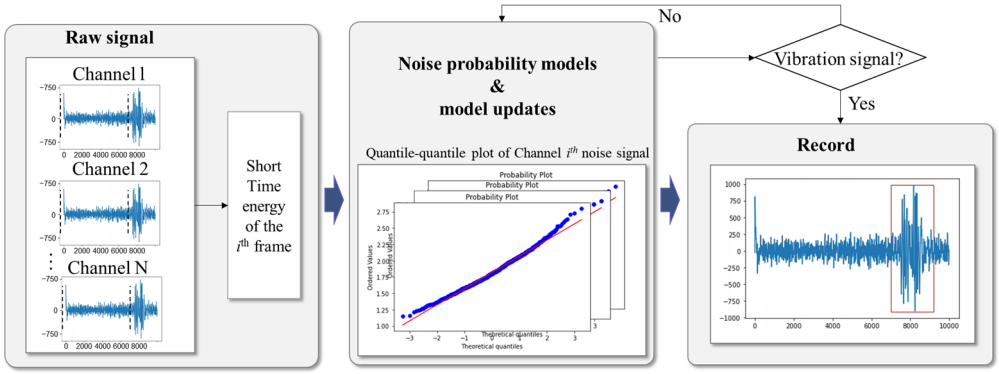

Figure 2. Vibration signal detection algorithm.

2.3. Axle Load–Time-History Reconstruction

In this paper, we estimated the axle load by reconstructing the load–time-history curve and calculating its peak value. This reconstruction task involved learning the relationship between the input vibration signal sequence and the output load sequence in a sequence-to-sequence manner. To achieve this, the input vibration signals and the output loads were synchronized in time, including the section before, during, and after the vehicle passes. In this study, the input sequence length was set to 700, which ensured that the complete vehicle signal was captured.

Let $\mathbf{X} = [\mathbf{x}^1, \mathbf{x}^2, \ldots, \mathbf{x}^N]$ denote a set of vibration signals, where xi is from the *i*th vibration sensor, and let **Y** denote the corresponding load–time-history curve. During the forward propagation step, a subset of **X** is fed into the TCN. The network then predicts the corresponding load–time-history curve, which is compared with the true load–time-history curve in the training dataset. The difference between them is computed as the error, which is then used to calculate the gradients. The weights of the TCN are updated using the gradients in a process called backpropagation. By repeatedly performing forward propagation followed by backpropagation, the weights of the network are adjusted to minimize the loss.

The proposed TCN network is presented in Figure 3. To increase the channels of the signals, a 1×1 convolutional layer is applied. The signals are then passed through a series of non-causal temporal blocks. The output of the final temporal block is concatenated with the input signals, and the predicted load–time-history curve is generated using a linear layer similar to U-net. Each temporal block comprises two layers of non-causal dilated convolutions, with batch normalization, non-linearity, and a dropout layer placed between them. The residual skip connection adds the input to the output feature map, with the caveat that if the input and output depth are different, a 1×1 convolution is inserted. Figure 3 illustrates a temporal block and the stacking of three residual blocks together. The first convolutional block (CONV) has N_T filters. There are N_B TCN blocks that use the same number of filters N_T, the same kernel length K_T, and a variable dilation $d \in \{1, 2, 4, \ldots, 2^{N_B}\}$. The default parameters are $N_T = 32$, $K_T = 31$, and $N_B = 12$.

To capture both high- and low-frequency contents, it is necessary to experiment with different kernel sizes and the number of temporal blocks to determine the optimal model. A larger kernel size with more layers enables the network to capture the low-frequency trend, while a smaller kernel size with fewer layers allows the network to capture the high frequencies.

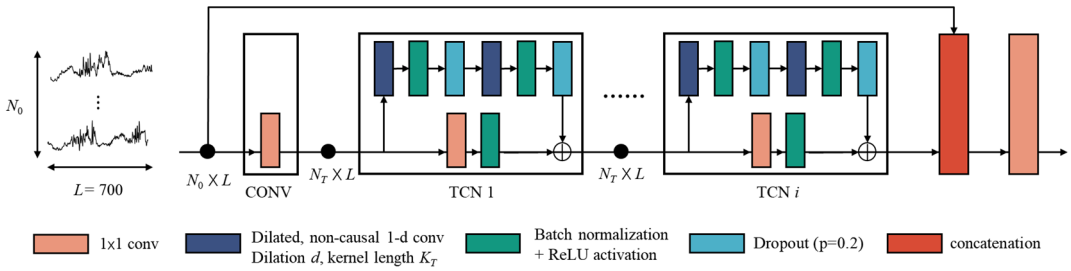

Figure 3. TCN architecture processing the number of vibration sensors (N_0) × 700 samples.

2.4. Training Strategies

Using the PyTorch environment, the model was developed, trained, and tested on an GeForce RTX 3060 GPU (produced by Nvidia, Santa Clara, CA, USA). In the training process, we optimized the network weights and biases using the mean square error loss (MSE) and uniformly initialized the filter kernels. To minimize the objective loss function, we used the Adam optimizer. The mini-batch size varied from 16 to 128 for different tasks. The initial learning rate was set to 1×10^{-4}, and we implemented adaptive adjustment of the learning rate. If the validation loss did not decrease for 15 epochs, we reduced the learning rate by a factor of 10.

2.5. Performance Metrics

To evaluate the generalization performance of the proposed methods, three criteria were introduced, as suggested by Chen et al. [25]: peak error (PE), main impulse error (MIE), and root mean square error (RMSE). PE was used to evaluate the performance of axle load value estimation, while MIE and RMSE assessed the ability of the model to fit low-frequency trends.

$$PE = \frac{1}{N}\sum_{i=1}^{N} \frac{\left|f_{\max}^{i} - \hat{f}_{\max}^{i}\right|}{f_{\max}^{i}} \times 100\% \tag{5}$$

$$MIE = \frac{1}{N}\sum_{i=1}^{N} \frac{\left|\sum_{t=T_1}^{T_2} f_t^i - \sum_{t=T_1}^{T_2} \hat{f}_t^i\right|}{\sum_{t=T_1}^{T_2} f_t^i} \times 100\% \tag{6}$$

$$RMSE = \frac{1}{N}\sum_{i=1}^{N} \sqrt{\frac{\sum_{t=T_1}^{T_3} (f_t^i - \hat{f}_t^i)^2}{\sum_{t=T_1}^{T_3} f_t^{i2}}} \times 100\% \tag{7}$$

where f denotes the actual load. Correspondingly, $\hat{f}$ represents the predicted load after mean filtering. N is the number of testing samples. T_1 is the start time of the one-axis impulse, and T_2 is the end time. As there are several axis impulses when a vehicle passes by, T_3 is introduced to signify the end time of the last axis impulse.

3. Field Testing

As described in this section, two field testing sites were used to assess the accuracy in estimating the rapid-moving load and natural vehicle load of concrete pavements. The concrete pavements at the two sites were designed to be different sizes, in order to study the effect of pavement size on the estimation.

3.1. Test Set-Up

3.1.1. Construction on Site

Site 1 and Site 2 were located in Shanghai, with Site 1 being situated at Tongji University and Site 2 at Zhengyu Road. Figure 4a illustrates the construction at Site 1, where a DOVS-based vibration sensing system was embedded 0.2 m beneath the surface of a

concrete pavement slab (4 m × 4 m × 0.25 m) using ten looped fibers, each with a diameter of 0.3 m. Additionally, a fiber Bragg grating (FBG) sensor was embedded into the concrete pavement to measure the dynamic strain. The FBG sensor was positioned under the mobile loading area at a depth of 0.22 m, and its orientation was along the direction of tire movement.

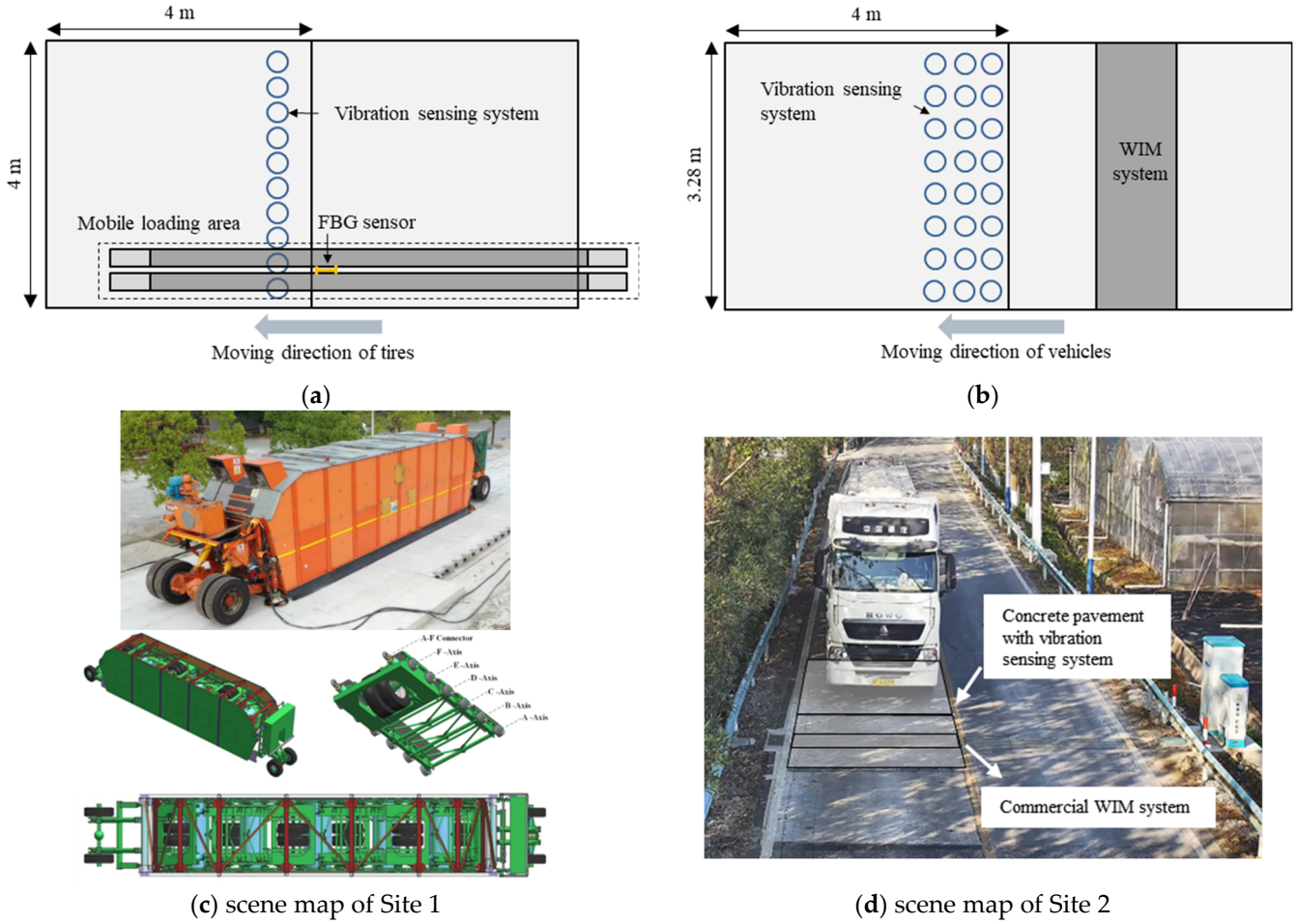

Figure 4. Test setup of the 2 test sites. (**a**) test set-up at site 1 (plan view); (**b**) test set-up at site 2 (plan view); (**c**) accelerated pavement testing equipment scene map of site 1; (**d**) scene map of site 2.

Figure 4b illustrates the construction at Site 2, located at Zhengyu Road, Shanghai. The DOVS-based vibration sensing system, consisting of twenty-eight looped fibers, was embedded into a concrete pavement slab (4 m × 3.28 m × 0.25 m). A commercial WIM system, OWS-ZWBH30 (produced by Mettler Toledo, Zurich, Switzerland), was also installed in the adjacent concrete pavement slab, as shown in Figure 4d.

3.1.2. Excitation

At Site 1, the pavement was excited by accelerating pavement testing equipment, MLS66 (produced by PaveTesting-MLS, Hertfordshire, UK), which provided repeated mobile loads. Figure 4c depicts the MLS66 and shows the axle configurations of the MLS66. The equipment has six axles, and each axle has two tires. These six axles continuously move when the MLS66 is running, applying up to 6000 passes of mobile loads per hour with controlled speed (maximum of 6 m/s), path, and magnitude (maximum of 75 kN). On the other hand, at Site 2, the concrete pavement was directly excited by traffic loads from moving vehicles, as shown in Figure 4d.

3.2. Data Collection

At Site 1, 15 test scenarios were conducted based on different speeds and magnitudes of mobile loads, as shown in Tables 1 and 2. The DOVS-based vibration system was used to measure concrete pavement vibration, while the FBG sensor was used to measure dynamic strain for each mobile load. The sampling frequency was set at 2.5 kHz, and the measured vibration and strain were recorded as a time history showing the variation during loading. This resulted in the collection of 2230 data samples. When pavement conditions were unchanged, the variation in mobile load applied at a specific position was proportional to the variation in dynamic strain measured at that position. Thus, the measured time history of strain for each data sample could be considered the ground truth for the time history of mobile load. After random windows were selected and down-sampled, a total of 6690 samples were obtained. The training set and the test set were divided by a ratio of 4:1. A uniform sampling of 80% of all load level and load speed samples was used as the training set to ensure a balanced sample distribution. Finally, the training set totaled 5352 samples and the test set totaled 1338 samples.

Table 1. Load scenarios at Site 1.

Load Level	No. 1 Axis (kg)	No. 2 Axis (kg)	No. 3 Axis (kg)	No. 4 Axis (kg)	No. 5 Axis (kg)	No. 6 Axis (kg)	Average Axle Load (kg)
1	2200	1690	1880	2020	2240	1750	1963.33
2	5150	4770	4910	5080	5250	4730	4981.67
3	6180	5120	5990	5830	6130	5630	5813.33
4	6700	6720	6900	6450	6990	5820	6596.67
5	7800	7080	7230	7470	7000	6900	7246.67

Table 2. Speed scenarios at Site 1.

No	Load Level	Loading Speed (m/s)	Percentage of Sample to the Total (%)	Number of Samples
1	1, 2, 3, 4, 5	2	15%	1004
2	1, 2, 3, 4, 5	4	40%	2676
3	1, 2, 3, 4, 5	6	45%	3010

Figure 5 presents the raw vibration signals and corresponding ground-truth mobile load signal during impact. It is observed that the fluctuation time range of the vibration signals is similar to that of the mobile load signal. The vibration signal amplitude increases as the load gets heavier and is more volatile as the loading speed increases too. This may be related to the amplitude of the dynamic response of the pavement influenced by external forces and loading rates.

At Site 2, the DOVS-based vibration sensing system measured vibrations induced by 335 vehicles on the concrete pavement with a sampling frequency of 2500 Hz. The axle configurations of these vehicles are shown in Table 3. When a vehicle passed by, the vibration sensing system measured the pavement vibration, and later, the commercial WIM system recorded the axle weights. These data were collected as samples. There were 335 data samples collected at Site 2. It should be noted that the ground truth of traffic loads should be in the form of time history, but the commercial WIM system was only able to provide a number representing the axle weight. Therefore, based on the recorded loading period, Gaussian distribution fitting was employed to expand the measured number to a time history. Then, the expanded time history was recorded as the ground truth of traffic loads. There were three rows of sensing loops that provided vibration data, and as they were close to each other, the ground truth of traffic loads was similar. Therefore, each row of vibration data was treated as an independent sample. The training set and the test set were also divided by a ratio of 4:1. The samples were evenly sampled according to vehicle type. The training set had 268 samples and the test set had 70 samples. After preprocessing

and augmentation, the number of training set samples was increased to 804 and the number of testing set samples was increased to 201.

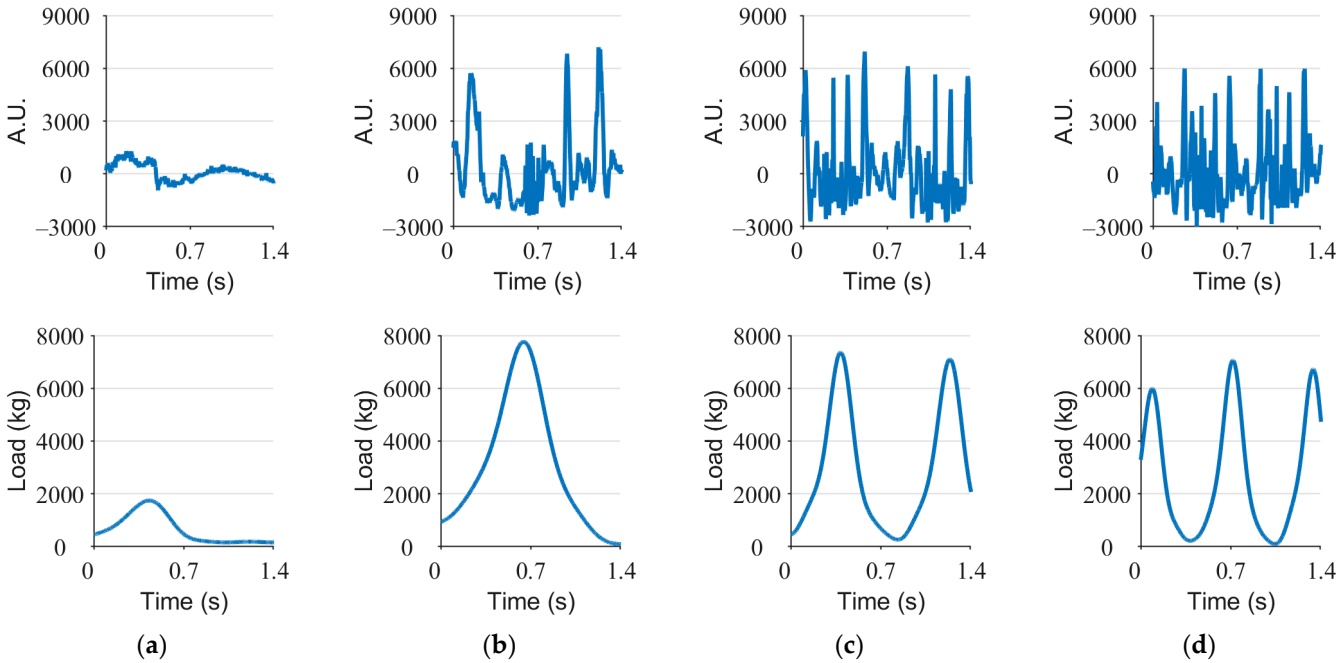

Figure 5. The history of the vibration signal measured from the sensing loop and the mobile load under the wheels. (**a**) speed = 2 m/s, load level 1; (**b**) speed = 2 m/s, load level 5; (**c**) speed = 4 m/s, load level 5; (**d**) speed = 6 m/s, load level 5.

Table 3. The axle configurations of vehicles.

No.	Vehicle Type	Axle Type	Percentage of Sample to the Total (%)	Number of Samples
1	Passenger car	1-1 *	46%	154
2	Lorry	1-1 *	12%	40
3	Truck-I	1-1 *	16%	53
4	Truck-II	1-2-2 *	26%	87

* Axle type 1-1 means both front and rear axles are single-axle. Axle type 1-2-2 means the front axle is single-axle while the two rearmost axles are dual-axle.

Figure 6 shows the raw vibration signals and corresponding ground-truth load signal as vehicles passed by. It can be seen that there is a positive correlation between vibration amplitude and vehicle axle load. Vehicle speed affects the calculation error of the axle load interval as shown in Figure 6d because of confusion of vibration signals generated by each axle. This may affect the accuracy of axle load estimation.

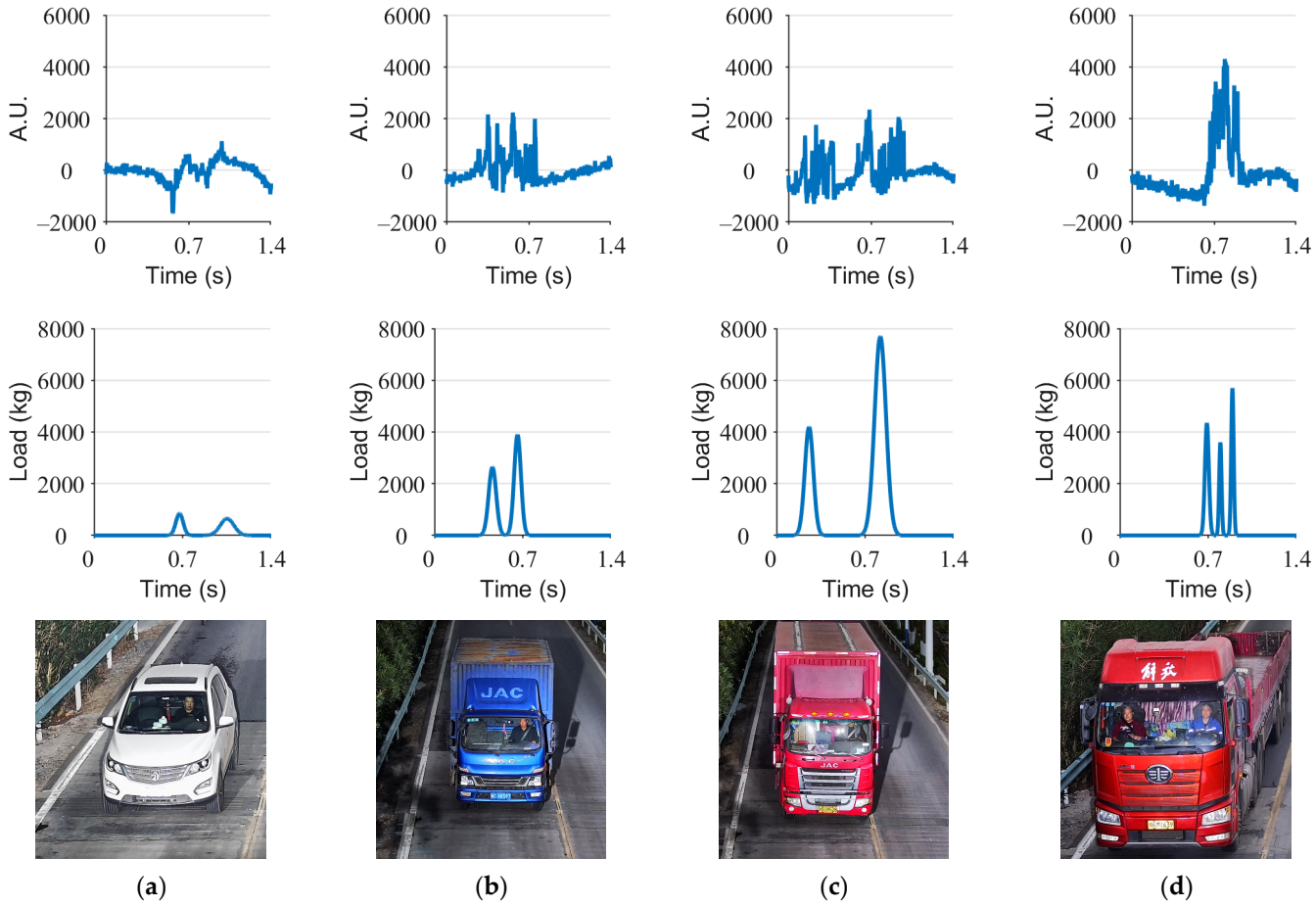

Figure 6. The history of the vehicle load and the vibration signal measured from the sensing loop under vehicles' wheels. (**a**) Passenger car; (**b**) Lorry; (**c**) Truck-I; (**d**) Truck-II.

4. Results and Discussion

To investigate the performance of the proposed method, the performance metrics of reconstruction for load–time history were first analyzed. Then, networks with different kernel sizes K_T and TCN blocks N_B were constructed to discuss the influence of the network architectures. Finally, the effect of speed on reconstruction results was discussed.

4.1. Reconstruction Results for the Load–Time History

The TCN load–time-history reconstruction network was constructed according to the structure presented in Figure 3, and the training strategy is as illustrated above. For Site 1, the length of the input sequences was 5×700, which corresponds to a signal duration of 1.4 s, using half of the sensing loop data. The TCN network reconstructed the time histories of 1338 test samples, whose speed and load were unknown in advance, using a batch size of 32. For Site 2, the length of the input sequences was 8×700, corresponding to one row of the sensing loop data. The TCN network reconstructed the time histories of 201 test samples whose vehicle locations were unknown in advance, using a batch size of 16.

To illustrate the results of the TCN identification method, the reconstructed impact loads of three samples from Site 1 and four samples from Site 2 are presented in Figures 7 and 8. The main impulse can be accurately reconstructed; however, some errors occur in the reconstruction of the peak so the capability of the model to capture high-frequency fluctuation features needs improvement in the future.

To quantitatively evaluate the performance of TCN, the peak error (PE), main impulse error (MIE), and root mean square error (RMSE) are calculated and compared in Figure 9. The results indicate that the proposed method achieves good performance for both Site 1

and Site 2. According to Equation (1), for both Site 1 and Site 2, all samples result in 11.5% PE, which is close to the errors allowed by the Long-Term Pavement Performance Program (LTPP) of 10% [1]. Compared to Site 1, the peak error is slightly increased and the RMSE is well behaved for Site 2. Since Site 2 is a practical scenario, it can be concluded that the proposed TCN model has good time-history reconstruction accuracy for axle loads under conditions of complex traffic.

The results indicate that the temporal convolutional network (TCN) model exhibits excellent load inversion accuracy for both sizes of cement concrete pavement. For Site 2, the TCN model demonstrated robust performance when subjected to natural traffic flow with varying speeds and vehicle types. Hence, it can be concluded that the TCN model performs well under different sizes of cement concrete pavement and varied load conditions. However, the current study lacks experimental design for asphalt pavement. In future research, we plan to expand the investigation to include asphalt roads to validate the model's performance in inverting loads from natural traffic flow on asphalt roads.

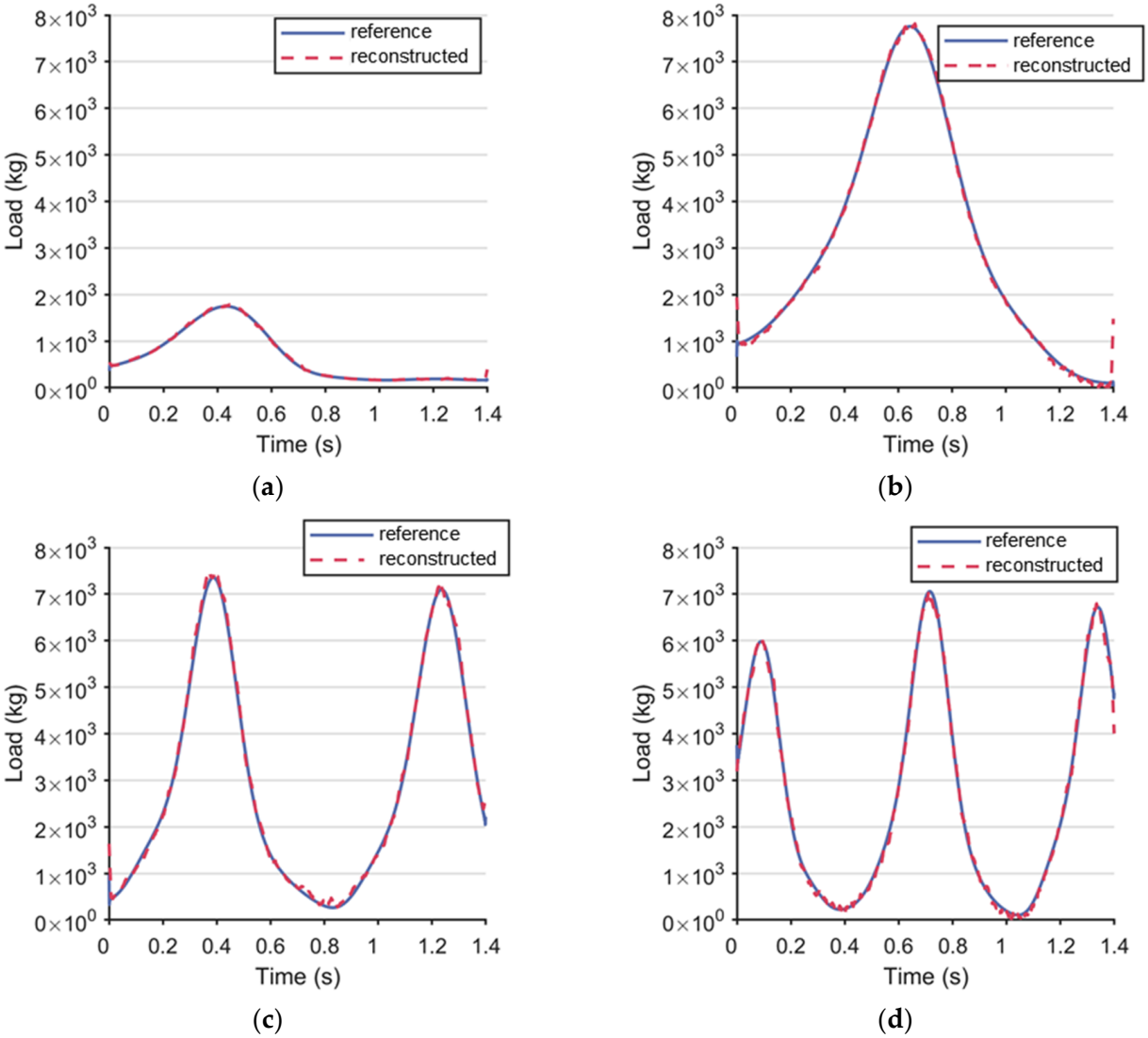

Figure 7. Site 1 reconstruction results. (**a**) speed = 2 m/s, load level 1; (**b**) speed = 2 m/s, load level 5; (**c**) speed = 4 m/s, load level 5; (**d**) speed = 6 m/s, load level 5.

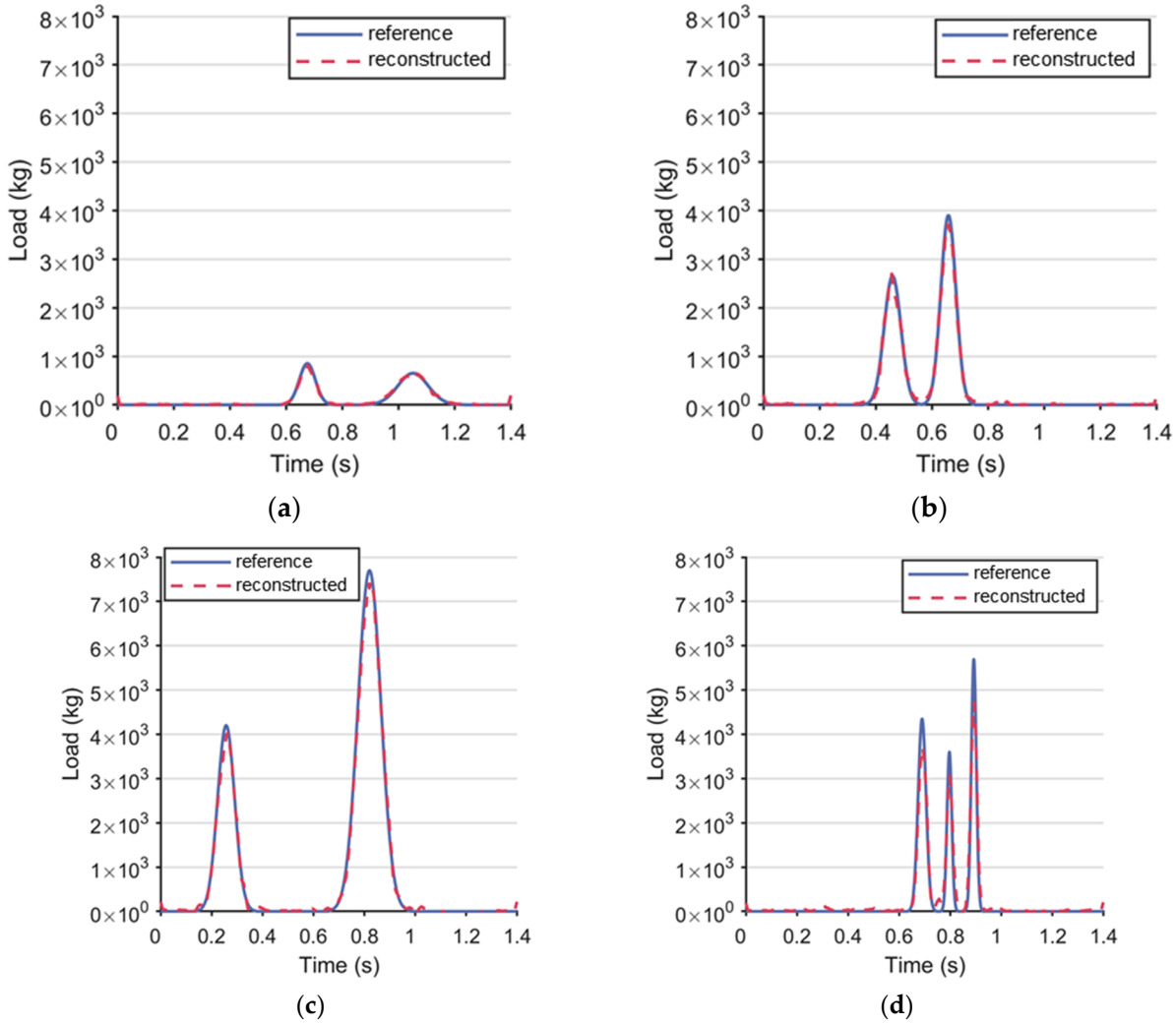

Figure 8. Site 2 reconstruction results. (**a**) Passenger car; (**b**) Lorry; (**c**) Truck-I; (**d**) Truck-II.

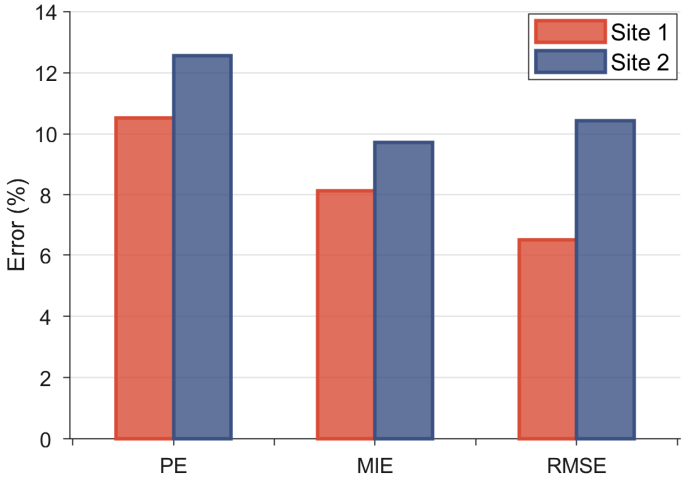

Figure 9. Performance of TCN model for load estimation.

4.2. Network Architectures

As previously mentioned, larger kernel sizes and more layers in the network capture low-frequency trends, while the network captures high frequencies. Therefore, we aim to compare the reconstruction performance of TCN networks with different kernel sizes

(K_T) and numbers of TCN blocks (N_B). As the network architecture's impact on the load reconstruction performance of various structures and load types is similar and the loads at Site 2 are more complex and closer to a real-world situation, this study only focuses on Site 2. We constructed and trained these networks with different hyperparameters, and the comparison results are presented in Figure 10.

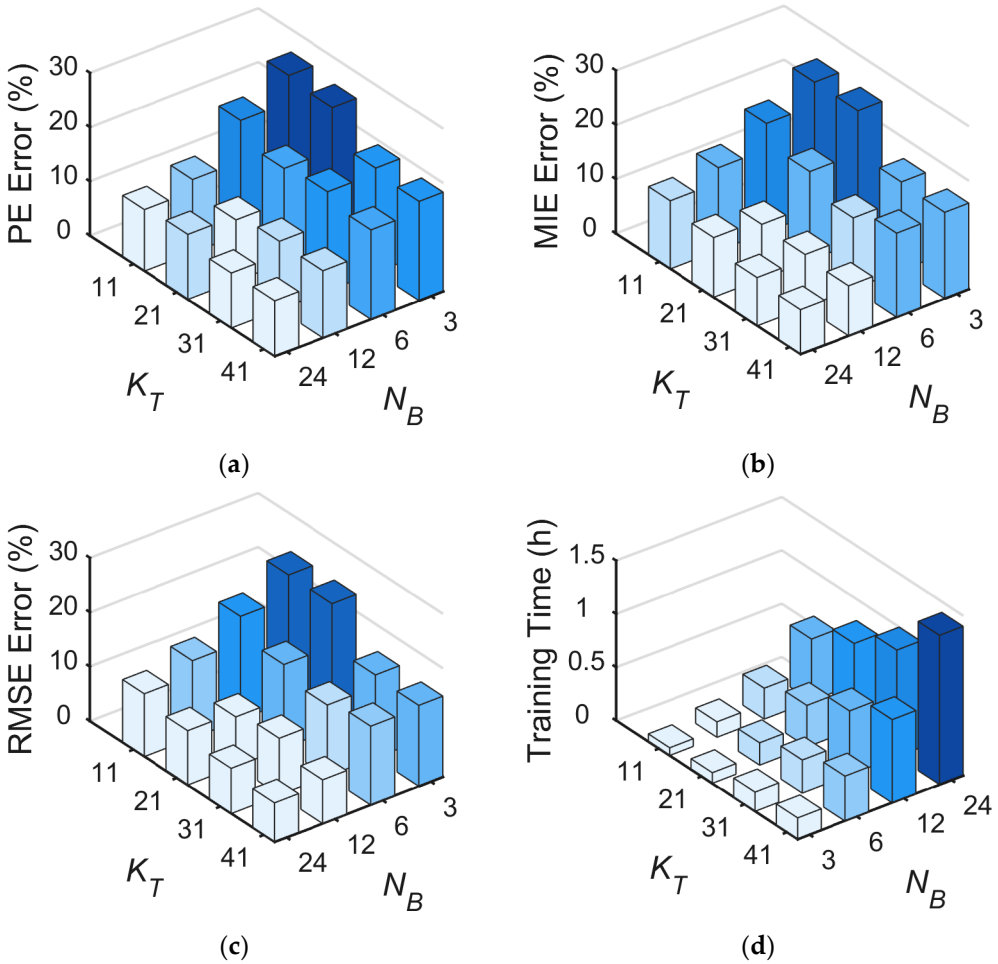

Figure 10. Performance of different network architectures for estimating axle loads. (**a**) PE; (**b**) MIE; (**c**) RMSE; (**d**) training time.

The peak and the axle impulse represent high-frequency and low-frequency features, respectively. Figure 10 illustrates that when utilizing a large value for N_B, the influence of K_T on recognition performance is diminished. Specifically, the value of K_T-21 results in a smaller PE compared to the values of K_T-31 and K_T-41 under N_B-12 while the opposite trend is observed for MIE. N_B, on the other hand, plays a vital role in reconstructing the impact load–time history, as the network's fitting ability increases with its depth. However, deeper layers require longer training times. Hence, we select the network with K_T = 31 and N_B = 12 as the optimal architecture, taking both factors into account. Finally, the mean estimation error, computed by averaging the values of PE, MIE, and RMSE, is found to be 10.89%.

4.3. Sensitivity Analysis of Speed

The amplitude and frequency of vibration in vehicle–road coupling are influenced by the speed of the axle load. Thus, the response of the sensor in the pavement is more affected by the vehicle's speed and the pavement's deflection level. We compare the reconstruction performance of the proposed method at various speeds, and Figure 11 illustrates the

distribution of sample speeds. The majority of the sample speeds are within the range of 2–10 m/s, which is a reasonable speed at the checkpoint.

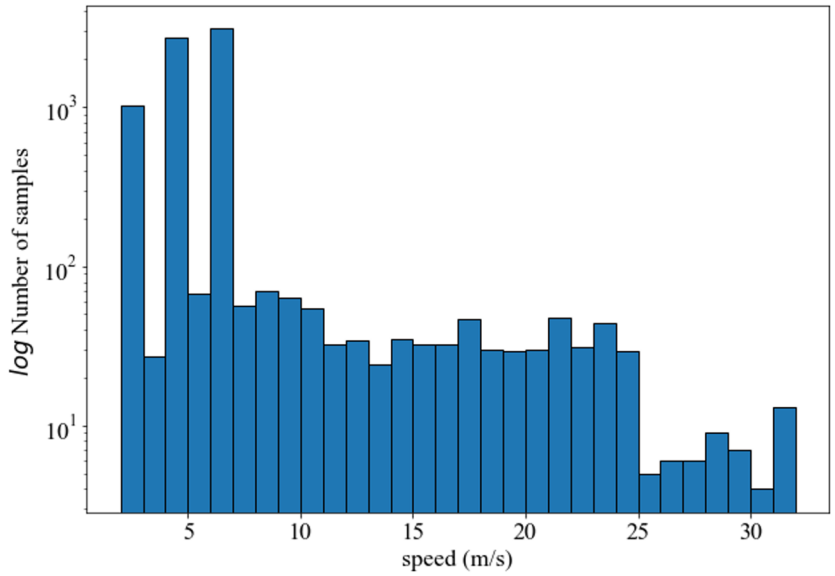

Figure 11. Speed distribution histogram.

Figure 12 shows the performance of the TCN model at different speeds. Intervals are established based on the speed distribution, with five intervals in total. There is a correlation between PE and speed, with PE being higher for speeds No. 1 and 5 compared to the other speeds. This is because faster speeds result in higher dynamic load factors, whereas slow speeds lead to weaker road vibration responses. When the signal-to-noise ratio is low in these cases, the vibration signal's peak feature may be overwhelmed by noise and, thus, become more difficult to detect. The PE of the proposed method remains small even in cases with low SNR, while there is not much change in MIE and RMSE. This observation reflects that the network captures low-frequency features effectively.

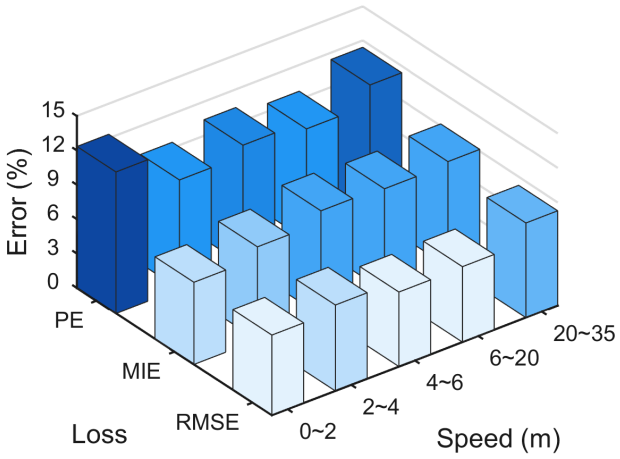

Figure 12. Performance of TCN model at different speeds.

4.4. Comparison with the Different Axle Load Estimation Methods

Table 4 shows results of the cost, error, and lifetime between different methods for axle load estimation [40]. The results show that the proposed method has advantages both in cost and lifetime. However, the accuracy is not as high as other methods.

Table 4. The axle configurations of vehicles.

Methods for Axle Load Estimation	Annual Life Cycle Cost ($)	Error	Expected Life (Years)
DOVS-based (presented)	1000	±11.5%	15
Bending plate	5000	±15%	4
Strip WIM (piezoelectric)	6000	±10%	6
Single load cell	8000	±6%	12

5. Conclusions and Future Work

Accurately measuring vehicle axle loads is a vital component in weight enforcement and pavement condition assessment. Existing WIM technologies are costly, impractical for high-speed vehicle detection due to inadequate time for pressure change registration, and susceptible to installation challenges. The goal of this paper was to develop an inexpensive but accurate DOVS-based WIM system. The vibration of concrete pavement contains valuable information that can identify vehicle load characteristics. But it is difficult to ensure the accuracy of the process, which typically requires complicated mathematical modeling and formula derivation.

The proposed method, characterized by an extended sensing range, high temporal sampling rate, and dense spatial sampling rate, demonstrates promising results in field tests under diverse conditions. The TCN model, trained with over 6000 samples of vibration data and corresponding ground truth of axle loads, exhibits the ability to learn the intricate inverse mapping between pavement structure inputs and outputs. The method achieves estimated axle loads within an 11.5% error margin, showcasing its efficacy in weight enforcement and pavement condition assessment. Furthermore, the approach aligns closely with specified standards such as those set by LTPP and Cost-323 [41], reinforcing its potential to offer valuable support in assessing and making decisions related to pavement structure conditions. The collection of pavement vibration data involves privileged data and is only used for traffic data analysis. The data have been desensitized and do not involve personal privacy.

Future work in this research avenue could focus on several aspects to further enhance the proposed method. Firstly, refining the deep learning-based load reconstruction method to accommodate variations in load conditions and pavement types would contribute to increased robustness. Secondly, exploring the application of the proposed methodology to asphalt pavements, which may present distinct challenges in coordination with fiber optic technology, could broaden its scope. Lastly, considering the potential integration of real-time monitoring capabilities into the proposed method would provide a dynamic approach to pavement assessment and management. Addressing these aspects would contribute to the continual improvement and applicability of the presented vibration-based method for axle load estimation in diverse pavement scenarios.

Author Contributions: Conceptualization, Z.B., M.Z. and H.Z.; methodology, Z.B. and M.Z.; validation, Z.B.; investigation, Z.B. and M.G.; resources, Z.B.; data curation, Z.B. and J.C.; writing—original draft preparation, Z.B.; writing—review and editing, Z.B., M.Z. and H.Z; visualization, Z.B. and M.G.; supervision, Z.B. and M.Z.; project administration, Z.B. and M.Z.; funding acquisition, H.Z. and M.Z. All authors have read and agreed to the published version of the manuscript.

Funding: This research was funded by the National Nature Science Foundation of China (Grant No: 52278457 and Grant No: 52308462) and Shanghai Pujiang Programme (23PJD043).

Informed Consent Statement: Not applicable.

Data Availability Statement: The data presented in this study are available on request from the corresponding author. The data are not publicly available due to privacy.

Acknowledgments: The authors thank the editor and anonymous reviewers for their numerous constructive comments and encouragement that have improved our paper greatly.

Conflicts of Interest: Author Juewei Cai was employed by the company Shanghai Research Institute of Building Sciences Co., Ltd. The remaining authors declare that the research was conducted in the absence of any commercial or financial relationships that could be construed as a potential conflict of interest.

References

1. *ASTM E1318-09*; Standard Specification for Highway Weigh-in-Motion (WIM) Systems with User Requirements and Test Methods. ASTM International: West Conshohocken, PA, USA, 2009.
2. Meyer, G.; Beiker, S. (Eds.) *Road Vehicle Automation*; Springer International Publishing: Berlin/Heidelberg, Germany, 2019.
3. Stokes, R.W. Weighing road vehicles in motion. *Meas. Control* **2006**, *39*, 244–247. [CrossRef]
4. Al-Qadi, I.; Wang, H.; Ouyang, Y.; Grimmelsman, K.; Purdy, J.E. LTBP Program's Literature Review on Weigh-in-Motion Systems. 2016. Available online: https://rosap.ntl.bts.gov/view/dot/35735 (accessed on 8 September 2023).
5. Tawfek, A.M.; Ge, Z.; Yuan, H.; Zhang, N.; Zhang, H.; Ling, Y.; Guan, Y.; Šavija, B. Influence of fiber orientation on the mechanical responses of engineering cementitious composite (ECC) under various loading conditions. *J. Build. Eng.* **2023**, *63*, 105518. [CrossRef]
6. Alavi, S.H.; Mactutis, J.A.; Gibson, S.D.; Papagiannakis, A.T.; Reynaud, D. Performance evaluation of piezoelectric weigh-in-motion sensors under controlled field-loading conditions. *Transp. Res. Rec.* **2001**, *1769*, 95–102. [CrossRef]
7. Jiang, X.; Vaziri, S.H.; Haas, C.; Rothenburg, L.; Kennepohl, G.; Haas, R. Improvements in piezoelectric sensors and WIM data collection technology. In Proceedings of the 2009 Annual Conference of the Transportation Association of Canada, Vancouver, BC, Canada, 18–21 October 2009.
8. Prozzi, J.A.; Hong, F. Effect of weigh-in-motion system measurement errors on load-pavement impact estimation. *J. Transp. Eng.* **2007**, *133*, 1–10. [CrossRef]
9. Zhang, C.; Shen, S.; Huang, H.; Wang, L. Estimation of the vehicle speed using cross-correlation algorithms and mems wireless sensors. *Sensors* **2021**, *21*, 1721. [CrossRef]
10. Stocker, M.; Silvonen, P.; Rönkkö, M.; Kolehmainen, M. Detection and classification of vehicles by measurement of road-pavement vibration and by means of supervised machine learning. *J. Intell. Transp. Syst.* **2016**, *20*, 125–137. [CrossRef]
11. Lajnef, N.; Rhimi, M.; Chatti, K.; Mhamdi, L.; Faridazar, F. Toward an integrated smart sensing system and data interpretation techniques for pavement fatigue monitoring. *Comput.-Aided Civ. Infrastruct. Eng.* **2011**, *26*, 513–523. [CrossRef]
12. Fan, W.; Qiao, P. Vibration-based damage identification methods: A review and comparative study. *Struct. Health Monit.* **2011**, *10*, 83–111. [CrossRef]
13. Ye, Z.; Xiong, H.; Wang, L. Collecting comprehensive traffic information using pavement vibration monitoring data. *Comput.-Aided Civ. Infrastruct. Eng.* **2020**, *35*, 134–149. [CrossRef]
14. Bajwa, R.; Coleri, E.; Rajagopal, R.; Varaiya, P.; Flores, C. Development of a cost-effective wireless vibration weigh-in-motion system to estimate axle weights of trucks. *Comput.-Aided Civ. Infrastruct. Eng.* **2017**, *32*, 443–457. [CrossRef]
15. Liu, P.; Xing, Q.; Wang, D.; Oeser, M. Application of dynamic analysis in semi-analytical finite element method. *Materials* **2017**, *10*, 1010. [CrossRef] [PubMed]
16. Wu, D.; Zeng, M.; Zhao, H.; Wang, Y.; Du, Y. Detection and localization of debonding beneath concrete pavement using transmissibility function analysis. *Mech. Syst. Signal Process.* **2021**, *159*, 107802. [CrossRef]
17. Hou, Y.; Li, Q.; Zhang, C.; Lu, G.; Ye, Z.; Chen, Y.; Wang, L.; Cao, D. The state-of-the-art review on applications of intrusive sensing, image processing techniques, and machine learning methods in pavement monitoring and analysis. *Engineering* **2021**, *7*, 845–856. [CrossRef]
18. Abedi, M.; Shayanfar, J.; Al-Jabri, K. Damage assessment via machine learning approaches: A systematic review. *Asian J. Civ. Eng.* **2023**, *24*, 3823–3852. [CrossRef]
19. Liu, J.; Sun, X.; Han, X.; Jiang, C.; Yu, D. Dynamic load identification for stochastic structures based on Gegenbauer polynomial approximation and regularization method. *Mech. Syst. Signal Process.* **2015**, *56*, 35–54. [CrossRef]
20. Huang, C.; Ji, H.; Qiu, J.; Wang, L.; Wang, X. TwIST sparse regularization method using cubic B-spline dual scaling functions for impact force identification. *Mech. Syst. Signal Process.* **2022**, *167*, 108451. [CrossRef]
21. Tang, H.; Jiang, J.; Mohamed, M.S.; Zhang, F.; Wang, X. Dynamic Load Identification for Structures with Unknown Parameters. *Symmetry* **2022**, *14*, 2449. [CrossRef]
22. Li, X.; Zhao, H.; Huang, J.; Chen, J. Force reconstruction for uncertain structure based on interval model and second-order perturbation theory. *Int. J. Comput. Methods* **2021**, *18*, 1950040. [CrossRef]
23. Movahedian, B.; Boroomand, B. Inverse identification of time-harmonic loads acting on thin plates using approximated Green's functions. *Inverse Probl. Sci. Eng.* **2016**, *24*, 1475–1493. [CrossRef]
24. Jiang, J.; Ding, M.; Li, J. A novel time-domain dynamic load identification numerical algorithm for continuous systems. *Mech. Syst. Signal Process.* **2021**, *160*, 107881. [CrossRef]
25. Chen, T.; Guo, L.; Duan, A.; Gao, H.; Feng, T.; He, Y. A feature learning-based method for impact load reconstruction and localization of the plate-rib assembled structure. *Struct. Health Monit.* **2022**, *21*, 1590–1607. [CrossRef]
26. Zhang, H.; Zhou, Y. AI-based modeling and data-driven identification of moving load on continuous beams. *Fundam. Res.* **2023**, *3*, 796–803. [CrossRef]

27. Zhao, H.; Wu, D.; Zeng, M.; Zhong, S. A vibration-based vehicle classification system using distributed optical sensing technology. *Transp. Res. Rec.* **2018**, *2672*, 12–23. [CrossRef]
28. Zeng, M.; Zhao, H.; Gao, D.; Bian, Z.; Wu, D. Reconstruction of Vehicle-Induced Vibration on Concrete Pavement Using Distributed Fiber Optic. *IEEE Trans. Intell. Transp. Syst.* **2022**, *23*, 24305–24317. [CrossRef]
29. Zeng, M.; Chen, H.; Ling, J.; Zhao, H.; Wu, D. Monitoring of prestressing forces in cross-tensioned concrete pavements during construction and maintenance based on distributed optical fiber sensing. *Autom. Constr.* **2022**, *142*, 104526. [CrossRef]
30. Zeng, M.; Wu, D.; Zhao, H.; Chen, H.; Bian, Z. Novel Assessment Method for Support Conditions of Concrete Pavement under Traffic Loads using Distributed Optical Sensing Technology. *Transp. Res. Rec.* **2020**, *2674*, 42–56. [CrossRef]
31. Zhao, H.; Zeng, M.; Chen, H.; Ling, J.; Wu, D. Investigating the effect of prestress force on cross-tensioned concrete pavement vibration. *Transp. Res. Rec.* **2020**, *2674*, 875–886. [CrossRef]
32. Liu, F.; Ye, Z.; Wang, L. Deep transfer learning-based vehicle classification by asphalt pavement vibration. *Constr. Build. Mater.* **2022**, *342*, 127997. [CrossRef]
33. Ye, Z.; Wei, Y.; Zhang, W.; Wang, L. An Efficient Real-Time Vehicle Monitoring Method. *IEEE Trans. Intell. Transp. Syst.* **2022**, *23*, 22073–22083. [CrossRef]
34. Zhou, J.M.; Dong, L.; Guan, W.; Yan, J. Impact load identification of nonlinear structures using deep Recurrent Neural Network. *Mech. Syst. Signal Process.* **2019**, *133*, 106292. [CrossRef]
35. Zargar, S.A.; Yuan, F.G. Impact diagnosis in stiffened structural panels using a deep learning approach. *Struct. Health Monit.* **2021**, *20*, 681–691. [CrossRef]
36. Qiu, B.; Zhang, M.; Li, X.; Qu, X.; Tong, F. Unknown impact force localisation and reconstruction in experimental plate structure using time-series analysis and pattern recognition. *Int. J. Mech. Sci.* **2020**, *166*, 105231. [CrossRef]
37. Liu, R.; Dobriban, E.; Hou, Z.; Qian, K. Dynamic load identification for mechanical systems: A review. *Arch. Comput. Methods Eng.* **2022**, *29*, 831–863. [CrossRef]
38. Bai, S.; Kolter, J.Z.; Koltun, V. An empirical evaluation of generic convolutional and recurrent networks for sequence modeling. *arXiv* **2018**, arXiv:1803.01271.
39. Yuan, S.; Lellouch, A.; Clapp, R.G.; Biondi, B. Near-surface characterization using a roadside distributed acoustic sensing array. *Lead. Edge* **2020**, *39*, 646–653. [CrossRef]
40. Wang, J.; Han, Y.; Cao, Z.; Xu, X.; Zhang, J.; Xiao, F. Applications of optical fiber sensor in pavement Engineering: A review. *Constr. Build. Mater.* **2023**, *400*, 132713. [CrossRef]
41. Jacob, B.; O'Brien, E.J. European specification on weigh-in-motion of road vehicles (COST323). In Proceedings of the Second European Conference on Weigh-in-Motion of Road Vehicles, Lisbon, Portugal, 14–16 September 1998; pp. 14–16.